ADVANCED MATERIALS TECHNOLOGIES
www.advmattechnol.de

Development and Evaluation of a Low-Cost LEGO 3D Bioprinter: From Building-Blocks to Building Blocks of Life

*Ahmad Moukachar, Katie Harvey, Eva Roke, Katherine Sloan, Cameron Pool, Shabbir Moola, Ameer Alshukri, Danielle Jarvis, Phoebe Crews-Rees, Grace McDermott, Lluan Evans, Jin Li, Christopher Thomas, Sion Coulman, and Oliver Castell**

The development of low-cost accessible technologies for rapid prototyping of mechanical components has democratised engineering tools for hobbyists and researchers alike. The development of analogous approaches to fabrication of soft-matter, and biologically compatible materials containing living cells, is anticipated to be similarly enabling across multiple fields of biological research. LEGO toy construction bricks represent low-cost, precision engineered, and versatile construction materials for rapid prototyping. This study demonstrates construction of a benchtop LEGO 3D bioprinter for additive layer manufacture of a 3D structure containing viable human skin cells within a hydrogel scaffold. 3D bioprinted structures are formed from the deposition of microfluidically generated bio-ink droplets containing live keratinocyte skin cells, representing components toward an artificial skin model. Fluid flow rates and printer speed, together with bio-ink gelation rate, determine droplet packing arrangement in the bioprinted structures. The printing of 3D structures containing multiple bio-inks is demonstrated and live cells are imaged in the resulting bioprints. Fluid delivery can be achieved using LEGO pumps and readily available, or home-3D-printed, microfluidic components, therefore avoiding the need for any specialist microfluidic hardware. Build instructions are described to enable easy uptake, modification and improvement by other laboratories, as well provide an accessible platform for learning and education. Affordable, accessible, and easy to use tools for 3D bioprinting are anticipated to open opportunities for a greater number of research labs to work with 3D cell culture and bio-printed materials, with bioprinting expected to assist in better understanding of disease, contribute to tissue engineering and repair, and enable personalised medicine through the printing of cultured patient cells. The presented approach is not only an easily accessible laboratory tool for bioprinting, but also provides a learning system for mechanical construction, robotics, coding, microfluidics and cell biology, making it a versatile platform for research, education, and science engagement.

A. Moukachar, K. Harvey, E. Roke, K. Sloan, C. Pool, S. Moola, A. Alshukri, D. Jarvis, P. Crews-Rees, G. McDermott, L. Evans, C. Thomas, S. Coulman, O. Castell
School of Pharmacy and Pharmaceutical Sciences
Cardiff University
Redwood Building
King Edward VII Ave
Cardiff CF10 3NB, UK
E-mail: castello@cardiff.ac.uk
J. Li
School of Engineering and School of Pharmacy and Pharmaceutical Sciences
Cardiff University
Queen's Buildings, The Parade, Cardiff CF24 3AA, UK

The ORCID identification number(s) for the author(s) of this article can be found under https://doi.org/10.1002/admt.202100868.

DOI: 10.1002/admt.202100868

1. Introduction

Technologies and approaches of the Fourth Industrial Revolution, which often fuse rapid prototyping, such as 3D printing, accessible automation, and robotics, decentralised manufacture, and biological engineering are providing rapid means to enhance multidisciplinary scientific research and provide a platform for transformative innovation. Accessible technologies such as 3D printing (also referred to as additive manufacture) for the rapid prototyping of mechanical components have enabled innovative new research methodologies and democratised engineering tools for chemical and biological research.[1] Mass-manufactured, precision-engineered, construction kits, such as LEGO, represent an extremely low cost, yet flexible, high tolerance, modular, and reconfigurable system for prototyping and building bespoke laboratory hardware and apparatus. Recent developments in commercial LEGO robotics (Mindstorms) and programable interfaces for control, enable the development of smart, or automated, systems at low cost and with minimal requirements of prior expertise. Such designs can easily be shared in open-design form, for global use or seeding further

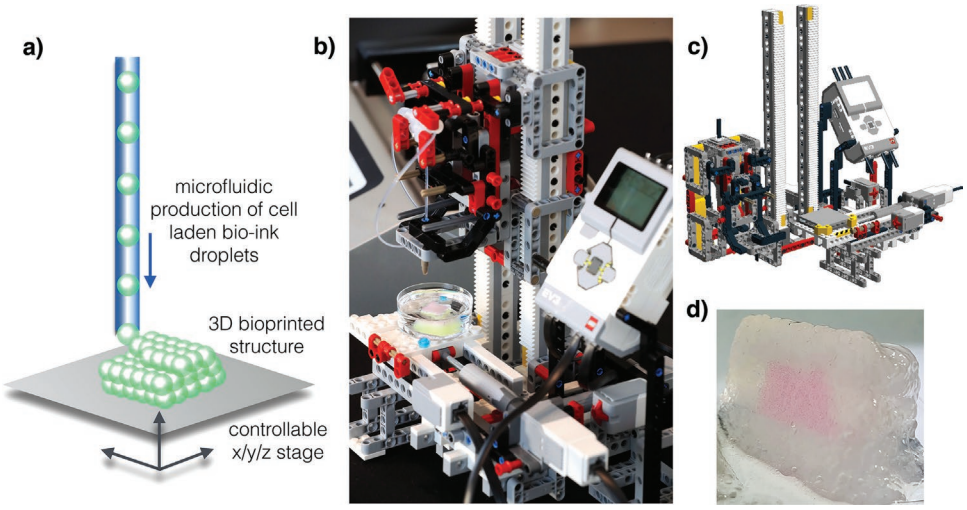

Figure 1. 3D Bioprinting Concept: a) Individual microfluidically produced droplets of cell-laden hydrogel bioink can be patterned in a 3D arrangement by controlled movement of an x/y/z-stage synchronized with droplet production. b) A 3D bioprinter is constructed from commercially available, LEGO (Technic and Mindstorm) precision, modular, construction-kit, with integrated microfluidic droplet generator assembled from commercially available ETFE T-junction and FEP tubing. c) LEGO CAD model of the 3D bioprinter build. d) Resulting 3D bioprinted structure fabricated with the system illustrated.

rapid iterative design improvements. To date, custom built LEGO tools used in scientific research have been reported in a number of research areas. Accurate tension sensors for characterising stretchable electronics have been reported, providing comparable performance to commercial machines.[2] Liquid-handling pipetting robots have been built,[3] and recently arrays of LEGO syringe drivers have been made for controlled reagent additions to live cells during microscopy imaging.[4] Microscope bodies,[5] and optics holders have also been reported.[6] The modular, reconfigurable format has also served as both inspiration,[7] and as a substrate for engineering microfluidic systems that can be easily modified and optimised by rearranging bricks in different combinations.[8] Thus far the focus of such LEGO hardware has been on engineering tools, often in disciplines already skilled in custom hardware manufacture and implementation. Translation of these tools, alongside principles of manufacturing of the Fourth Industrial Revolution, to areas of soft-matter and biological research can introduce otherwise inaccessible, low cost, open-platforms, and tools to an arena with a current paucity of accessible options for researchers either without considerable funding resource or in-house engineering expertise.

Here we report the design, build and implementation of a LEGO-built 3D bioprinter for the printing of live-cells in 3D-printed hydrogel structures suitable for 3D tissue culture. 3D bioprinting is an emerging field that uses 3D deposition techniques to build cell-laden, tissue-like structures, layer-by-layer into 3D designs, with control of cellular patterning and spatial arrangement.[9–12] Increasingly, 3D bioprinting methods seek to include biocompatible scaffold materials, vascularized systems, chemical reagents or growth factors to increase the sophistication of bioprinted tissue models.[13–17] Such 3D bioprinting methods and materials provide major opportunities to enhance tissue and organ models by creating a 3D environment that is more representative and authentic than traditional 2D cell culture models. Thus, they are of significant interest to those striving to understand biological processes at the cellular, tissue and organ levels, in both the healthy and diseased state, and for the evaluation of novel therapies.[18–20] In the longer-term, 3D-bioprinting is expected to assist more widely in tissue engineering and repair,[21] and in personalized treatments by an autologous cell-printing approach.[22] Similar to the step-change in capability afforded by traditional 3D printing with affordable off-the-shelf printers, low cost, accessible 3D bioprinting is anticipated to have a similar impact in biological research. The ability to create 3D culture systems with defined structures, spatial cell patterning and the ability to perfuse with artificial vasculature will create a step-change in research capability compared to traditional 2D cell monoculture.[15,17,24,25] To facilitate wider uptake and development of 3D bioprinting in biological research labs, even for use in relatively simple tasks, such as better understanding of 3D cell culture,[25] the tools for 3D bioprinting need to be affordable, accessible, and easy to use.

Here, we present the first use of LEGO applied to soft matter 3D printing to create a programmable 3D bioprinter. We report the construction of a programmable LEGO x,y,z platform with integrated droplet microfluidic nozzle(s) for the controlled spatial deposition of live cells encapsulated in discrete droplets of hydrogel bio-ink. Chemical gelation of the bio-ink upon 3D printing serves to gelate larger 3D structures built from individually deposited hydrogel droplets. In this way, we demonstrate the ability to build 3D printed biomaterials, patterning live-cells of different identity within a 3D tissue like structure that is characterized by wide-field microscopy, confocal microscope, and light-sheet imaging.

2. Results and Discussion

2.1. Development of an Integrated LEGO 3D Bio-Printer

The reported 3D bioprinter is easily assembled from LEGO and commercially available fluidic fixtures and fittings, creating an

easily replicable and affordable 3D bioprinter (**Figure 1**). The printer has a range of motion of 40 mm in x and y directions and the option to control printing nozzle height over a range of 150 mm. x/y/z printing precision for deposition of droplets is defined by the droplet diameter and the bioprinter step-size, here nominally ≈4.15 µm in x/y and 70 µm in z. Droplet size is readily controlled by the microfluidic tube or channel geometry and input fluid flow rates. We report the ability to use custom fused-filament 3D-printed LEGO-style fluidic modules or simple commercially available FEP tubing (I.D. = 750 µm) and Tefzel T-pieces (I.D = 500 µm) to construct the microfluidic delivery components of the bioprinter. Fluid delivery can be made by either commercially available syringe drivers or previously reported LEGO syringe drivers (Supporting Information).[4] The total cost of the bioprinter is £350 using LEGO pumps or £1500 with commercial syringe drivers, making it a readily accessible platform to researchers in most laboratories. LEGO bricks are mass fabricated with a high degree of precision (tolerance 0.002 mm),[26] enabling repeatability in builds. The printer is able to print in multiple bio-inks by using either multiple fluidic nozzles in parallel, or by the use of sequential fluidic inlets into a common nozzle, with printing performed directly into a cell-culture petri-dish. The bioprinter frame and x/y position stage are built from a combination of LEGO Mindstorms programmable robotics LEGO and Technic LEGO (Figure 1; Figure S3 and Video S1, Supporting Information), with the x/y stage design informed by a previously reported LEGO mechanical stage for polymer filament writing from a commercial extrusion pen.[53] The LEGO Mindstorms control brick (LEGO Mindstorms EV3 Intelligent Brick 45500) is programmable and controllable via LabView (National Instruments) or a stripped-down Mindstorms specific LabVIEW-based software programming environment which is free to use. 3D printed design programs can be run either directly from the Mindstorms brick in standalone mode, from a control PC connected via USB, or from a phone or tablet via Bluetooth. Touch sensors inform the printer of an initial x/y/z position that allows spatial calibration to a user defined origin, from which printing can be initiated. Servo motors control movement of the x/y stage and the z-height of the microfluidic printer nozzle. The EV3 Large Servo Motor used to control the printer stage movement affords a movement accuracy and minimum movement of one degree rotation. With the actuator coupled to stage movement, this translates to a stage movement of ≈4.15 µm per degree rotation of the servo motor (Figure S1, Supporting Information). Nozzle positional accuracy demonstrated high return position reproducibility with a standard deviation of +/− 30.6 µm (**Figure 2**e; Figure S2, Supporting Information). The microfluidic delivery of cells is achieved using droplet microfluidics, to create a stream of individual cell-laden alginate droplets.[7,27] By moving the x/y stage at a rate proportional to the rate of droplet production, continuous deposition of contiguous droplets in pre-determined 2D patterns is possible by building up such 2D patterns sequentially, layer-upon-layer, 3D patterns can be achieved by creating 3D bioprinted structures containing live cells within a hydrogel scaffold (Figure 1).

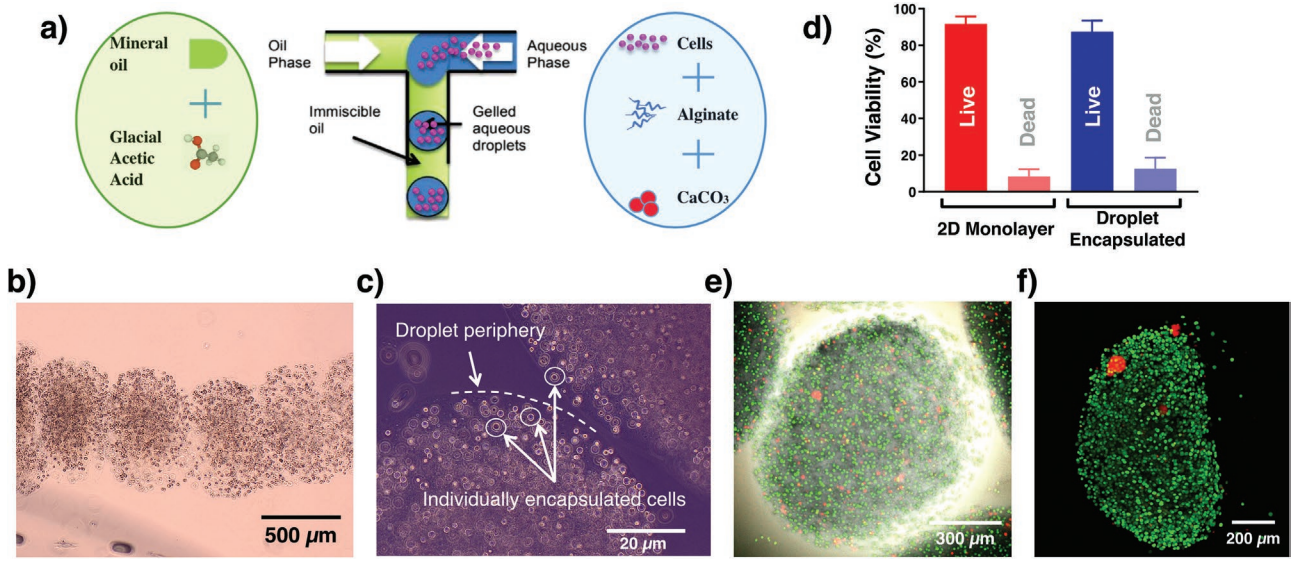

Figure 2. Generation of 3D patterned structures: a) Mindstorms visual programming language allows motor and sensor sequences to be wrapped into blocks with input and output functionality such that parameterisation can control motor speed, x/y/z shape traced and therefore determine layer-by-layer 3D print designs. b) LabVIEW interface for alternative operation. c) Example of layer-by-layer stage movement instructions to build a two-bioink design of an encased cube. d) Schematic of experimental setup to execute dual-bioink printing of an encased cube. Two alternative bioinks may be independently delivered to the microfluidic droplet generating T-junction to enable a print using two, or more, different bio-inks. e) Resulting dual bioink printing of a cube (containing pink fluorospheres) encased within a larger cube (without pink fluorospheres). f) sectioning of the final printed material to highlight the internal encased cube structure. g) Readily available microfluidic ETFE T-junction, used to generate the printed droplets, mounted on the LEGO bioprinter. h) Fused-filament 3D-printed cyclic olefin copolymer (COC) microfluidic droplet generator fabricated in a LEGO compatible brick design that can alternatively be integrated directly into the LEGO bioprinter build. e) Nozzle positional reproducibility following a programmed x,y,z movement series for repeat runs operated over the course of 7 days.

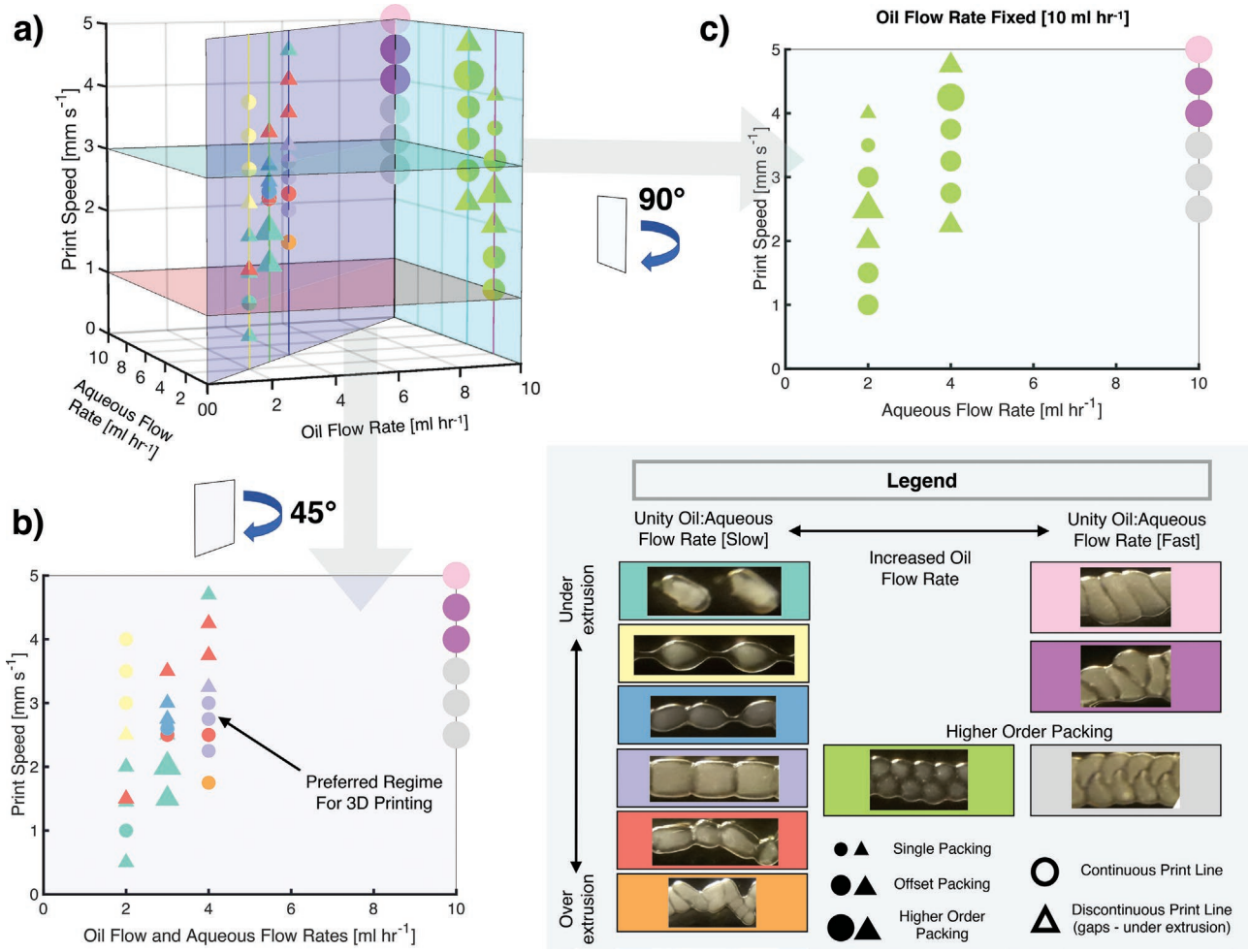

Figure 3. Microfluidic encapsulation of live cells: a) Microfluidic approach to cell encapsulation in droplets and gelation of the hydrogel bioink: Immiscible flows of liquid alginate and mineral oil meet at a microfluidic *T*-junction. The dominance of viscous and surface forces at this scale gives rise to regular hydrogel droplet formation encapsulating live cells suspended in the hydrogel phase. In the droplet flow regime glacial acetic acid dissolved in the mineral oil partitions into the aqueous hydrogel phase, transiently reducing the pH to liberate calcium ions from calcium carbonate nanoparticles suspended in the liquid hydrogel, subsequently cross-linking and gelling the alginate bio-ink. Reagent concentrations, fluid flow rates, fluidic geometries and droplet transit time, all influence the rate and extent of gelation. b) Linear movement of the x/y stage deposits a contiguous line of bioprinted droplets, c) each containing encapsulated live HaCaT cells. d) Trypan blue exclusion cell viability assay shows comparable cell viability following 3D printing to surface-seeded 2D monolayer ($n = 3$). e) Confocal microscopy of a single bioprinted droplet showing the dispersion and quantity of live (green) and dead (red) cells. f) Light-sheet 3D imaging of a single bioprinted droplet that has been excised from a linear bioprint and mounted in a glass capillary. Live (green) and dead (red) cells are illustrated.

2.2. Characterising Microfluidic Cell-Encapsulation

Liquid alginate droplets containing live cells are prepared by combining an aqueous gel flow with a second flow of immiscible mineral oil at a microfluidic T-junction. The dominance of surface and viscous forces on the microscale drives droplet break-up,[28] which in a hydrophobic channel, results in a flow of monodisperse gel droplets within a continuous oil flow. Using a previously reported approach,[7,27,29,30] acetic acid is incorporated into the mineral oil phase and calcium carbonate suspended in the alginate aqueous phase. Upon the two phases meeting within the microfluidic system, acetic acid partitions into the aqueous phase, a process accelerated by the internal recirculatory flow that manifests within droplets of microfluidic segmented flow regimes.[31,32] This gradually reduces the local pH, liberating calcium from the calcium carbonate that cross-links, and subsequently gels the alginate. By modulating the relative concentrations of acetic acid and calcium carbonate, particle size, fluid flow rates, flow ratios and droplet transit time, the extent of gelation on droplet exit from the microfluidic nozzle may be controlled. By depositing the extruded droplets into a reservoir of mineral oil the acetic acid is rapidly diluted, quenching further gelation and limiting the temporal exposure of the encapsulated cells to the lower pH environment. **Figure 3**a illustrates this process schematically. HaCaT keratinocyte cells (purchased from ATCC) were incorporated into the hydrogel bio-ink with a view to fabricating a 3D skin model. LIVE/DEAD cell staining with fluorescent imaging 2 h post-printing revealed homogeneous dispersion of viable HaCaT cells within individually printed droplets. Under

printing conditions of alginate and oil flow rates of 4 ml hr^{-1}, droplets were generated at a frequency of 3.4 droplets s^{-1} for ≈13.5 s and deposited in a straight print line. Under these conditions, droplets generated were typically 330 nl in volume, with each droplet containing ≈3300 cells (Figure 3). 3D printed droplet structures were printed into cell culture wells. By printing directly into a mineral oil layer, the sterility of the bioprint can be preserved before transferring for buffer exchange and incubation. Following printing, the alginate scaffold can be de-gelled and dissolved by chelation of calcium with Ethylenediaminetetraacetic acid (EDTA).[33,34] Thus, 250 mM EDTA was added to the bioprinted structure for 15 min, before dilution with DMEM, collection and centrifugation for cell recovery and analysis. A trypan blue exclusion cell viability assay indicated that 87.5% of cells remain viable during this process ($n = 3$). As a comparator, a conventionally seeded 2D HaCaT monolayer was detached with trypsin (0.25%)-EDTA (0.9 mM) with a 15 min incubation, before an equivalent cell reclamation procedure and trypan blue assay, which measured a 92% cell viability (Figure 3) ($n = 3$). An estimated 202 500 cells were contained in the assayed 3D bioprints, with 2D monolayers providing an average of 147 500 cells. These findings show that cell viability is maintained during the printing processes and upon short exposure to EDTA, whilst alginate de-gelation takes place. The addition of sodium citrate could provide a comparable alternative route to alginate dissolution (Figure S4, Supporting Information).[35] These methods provide a route to achieve selective cell deposition by scaffold dissolution, which could seed cells on surfaces, or deposit cells selectively within a multi-ink bioprint where dissolution of some gel matrix droplets takes place, whilst others remain.

2.3. Optimising Bio-Printing Parameters to Control Droplet Packing

The rate of droplet generation was systematically modulated alongside the speed of 3D printer stage movement to achieve optimal droplet deposition for production of 3D shapes (**Figure 4**b). For the alginate bioink system described here, alginate and oil flow rates each of 4 ml hr^{-1} gave rise to a droplet production frequency of 3.4 droplets per second where a lateral stage movement speed of 2.75 mm s^{-1} produced closely packed droplet structures upon printing. At this flow rate a 9 cm exit tube length provided a droplet transit time of ≈19.9 s before deposition; this provided a sufficient level of gelation to retain droplet structure, but sufficient fluidity to ensure coalescence of contacting droplets upon printing. This facilitated fusion of droplets into a single contiguous multi-droplet structure (Figure 4). An imbalance of printer stage speed and droplet production frequency manifests in under- or over-extrusion, which could take several forms, in part due to the complex interplay of variables affecting droplet size, acetic acid partitioning and mass transfer, droplet transit time, extent of alginate gelation, and droplet spacing on printing.[36,37] At equal flow rates of alginate and oil, with systematically varied printer stage speed, broken discontinuous droplet chains (Figure 4 – triangles), or slightly buckled packing, were observed when the printer stage speed was marginally too fast or too slow, respectively. At more extreme printer stage speeds, at the same droplet generation frequency, individually spaced or pearl-chained droplet chains were printed. Increasing oil flow rate to 10 ml hr^{-1} served to increase droplet production frequency across a range of aqueous flow rates (2–10 ml hr^{-1}) and reduced droplet size. This enabled droplet deposition in alternative packing regimes of horizontally "squeezed" and aligned "slugs" of material, interdigitating teardrops and offset double-row packing (Figure 4c – Higher Order Packing). These different packing regimes could ultimately be used to pattern printed materials in different ways, providing different structural features.

2.4. Generating High-Resolution Patterned 2D and 3D Structures

LabVIEW code was scripted that enabled x/y stage tracing of custom-defined shapes that translate to x/y stage movement determining the locations of droplet deposition. The layer-by-layer deposition of sequential 2D layer droplet arrangements is used to build a 3D structure with sub-mm resolution (Figure 2). The print head nozzle is programmed to rise incrementally (0.82 mm) following the deposition of each layer in order to maintain approximately consistent droplet drop-height and prevent the nozzle clashing with preceding layers. In this way the LabVIEW code readily translates a sequence of user defined 2D shapes with control over the x/y/z location into a layered 3D build. At a flow rate (total flow 4 ml h^{-1}) and droplet volume of 330 nl, with a gel phase comprising 2% alginate (w/v) with 7.5 mg mL^{-1} suspended calcium carbonate, and a mineral oil phase containing 0.5% glacial acetic acid (v/v), using a droplet outlet tube length of 9 cm, droplets were deposited in a closely packed formation that gelled to create a contiguous structure (Figure 4). Figure 2 depicts the printing process and the conceptual approach to coding the LabVIEW control programme. This control interface enables flexible operation for the printing of custom designed structures for users without coding experience (Figure 2; Figure S6, Supporting Information). Multi-material printing may be achieved using multiple parallel nozzles, or sequential control of multiple input fluids into a common droplet generator and single nozzle (Figure S2, Supporting Information). The ability to synchronize stage-movement of the bioprinter with microfluidic pump control was demonstrated by switching bio-ink during printing to enable printing of multiple cell types, or different bio-inks, within a single structure. This approach is illustrated in Figure 2e,f, where an inner cube of fluorosphere containing gel droplets is patterned within an outer structure of "blank" hydrogel droplets and exemplifies the printer's ability to construct 3D patterned shapes that are built from multiple pre-defined 2D deposited layers.

2.5. 3D Bio-Printing of Patterned Structures Containing Live Cells

Figure 5 depicts a bioprinted cuboid structure comprised of 18 sequentially printed 16 mm squared lattice structures (two orthogonal layers). Alginate bio-inks containing green and carmine fluorescent microspheres, in addition to blank alginate

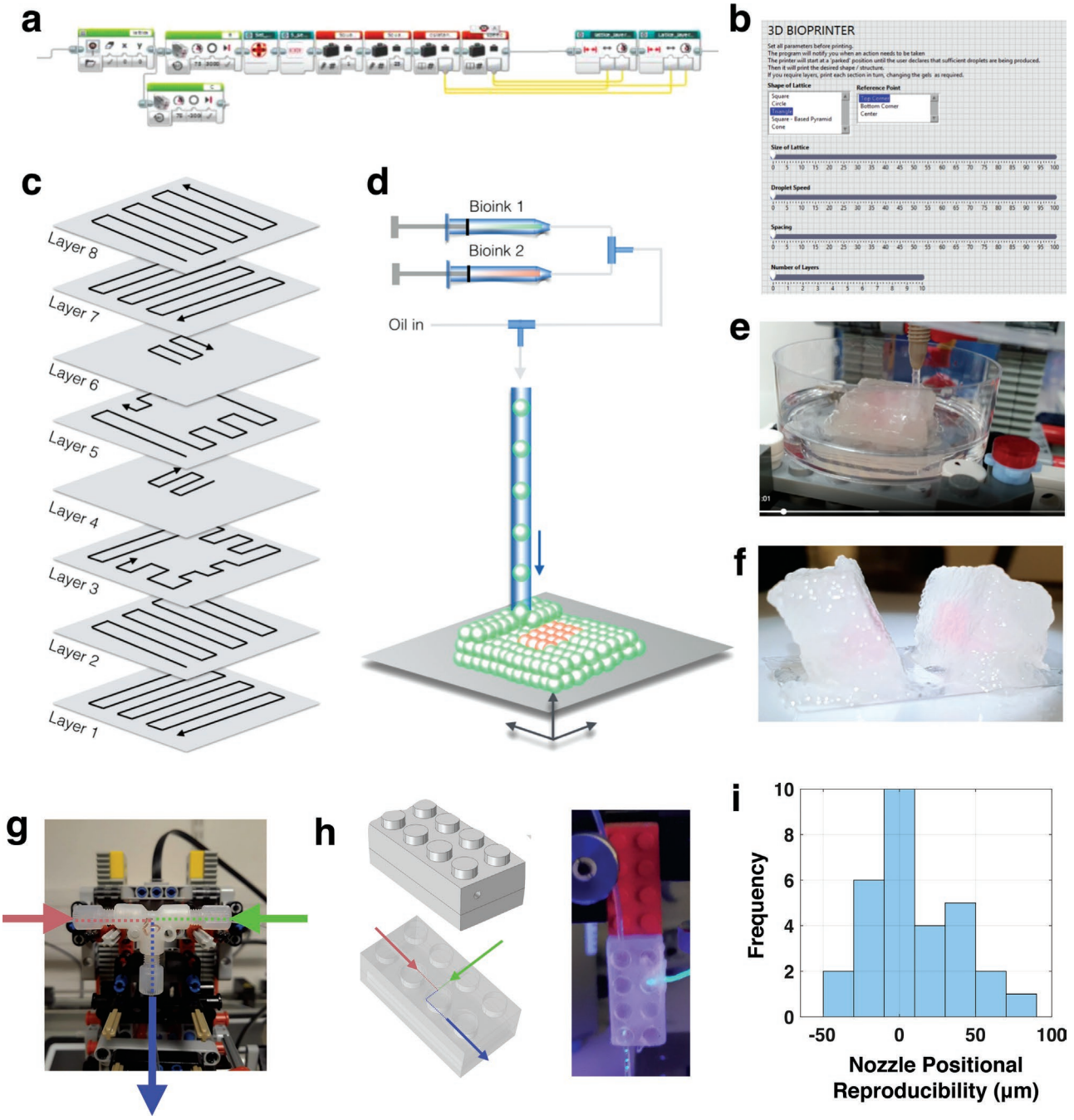

Figure 4. Aqueous and oil flow rates together with printer movement speed determine droplet patterning: a) Observation of droplet packing arrangements on exploration of a range of b) equal flow ratio (hydrogel and oil flows = 2.0–10.0 mL hr^{-1}) across a range of printer stage movement speeds (0.5–5.0 mm s^{-1}) and c) higher fixed oil flow rate (10 mL hr^{-1}) with variation of hydrogel flow rate (2.0–10.0 mL hr^{-1}) across a range of printer stage movement speeds (0.5–5.0 mm s^{-1}). Marker colors represent observed printed droplet patterning (see legend), circular markers represent printing of contiguous droplet structures, with triangular markers representing discontinuous printed arrangement. Surface tension and extent of gelation drives droplet association, discontinuities arise periodically where printer movement speed exceeds deposition rate (under extrusion), regular pearling or stretched contacts are also observed in some stable under-extrusion regimes. Over-extrusion results in concertinaing before emergence of higher-order packing arrangements. Absolute flow rates, phase ratio and reagent concentration influence droplet generation frequency, droplet size and also extent of gelation which all influence droplet packing together with printer speed. Oil and aqueous flow rates each of 4.0 ml hr^{-1} with a printer movement speed of 2.75 mm s^{-1} was deemed optimum for 3D bioprinting, producing contiguous square packed droplets.

bio-ink, were incorporated into three tiers within the 3D structure (Figure 5). Here, fluorescent microspheres were incorporated as model cell-sized objects that can be easily visualized on both the macro- and micro-scale. Vertical sectioning of the 3D-printed structure shows internal maintenance of the layered pattern, which is characterized by fluorescence microscopy

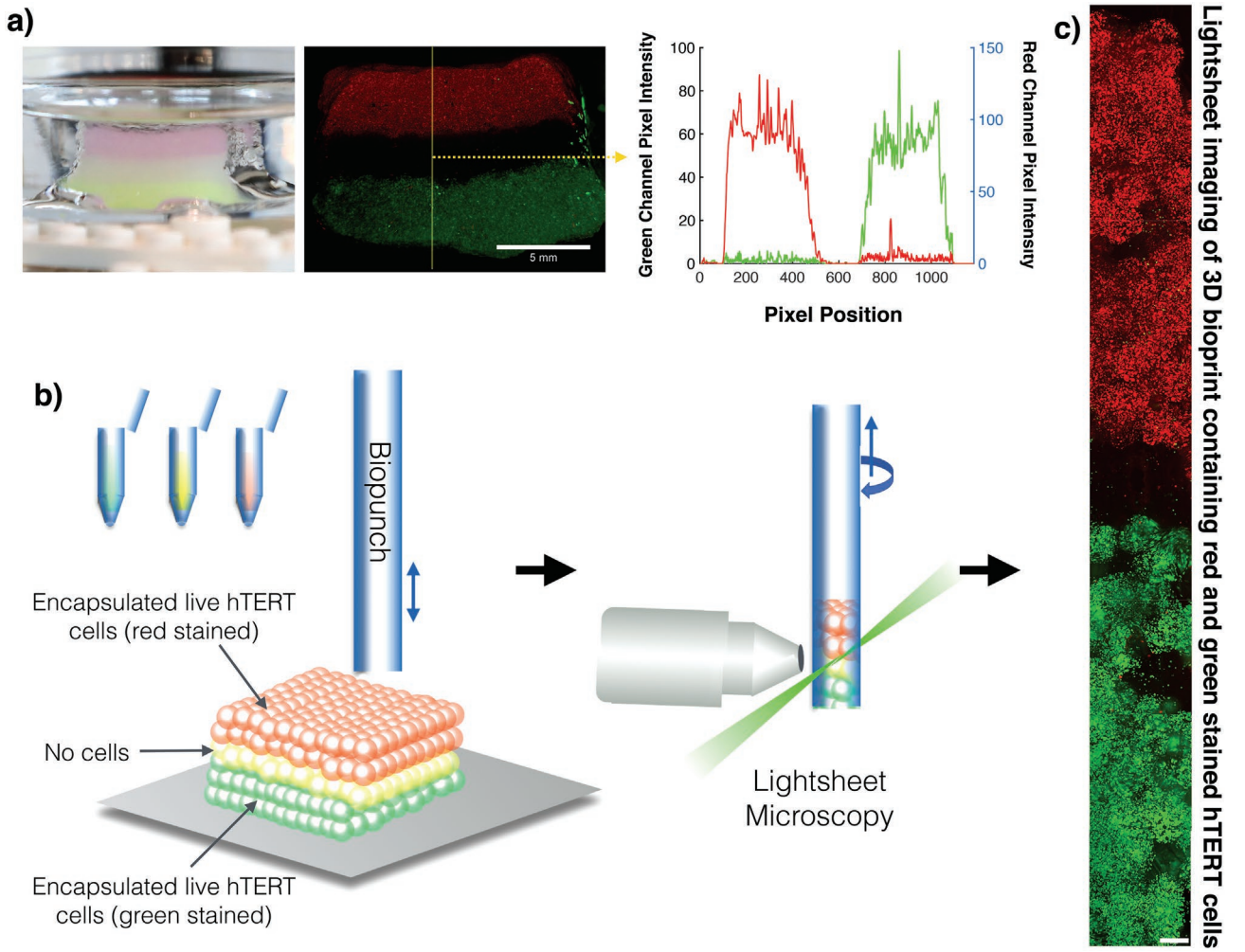

Figure 5. Multi-material bioprinting with encapsulated live hTERT/KER-CT cells imaged by light-sheet microscopy: a) A three-bioink multi-layer lattice print with bio-ink layers containing cell-sized green fluorospheres (8-layers), no fluorospheres (4-layers) and red fluorospheres (6-layers). Macroscopic fluorescent imaging of the sectioned bioprint shows encapsulated fluorospheres located in the 3D bioprint. This is quantified in the red and green channel image pixel intensity across the structure (see: graph). b) Schematic illustration of 3D bioprinted structure comprised of three bioinks containing no cells or suspended live hTERT/KER-CT cells with membranes stained with green, or red, fluorescent cellmask. The resulting structure is biopunched with a glass capillary to excise a sample tissue section for 3D light-sheet fluorescent imaging. c) Light-sheet microscopy of excised section of 3D bioprinted structure with maintenance of stained cell positioning within the 3D printed architecture (scale bar = 500 μm).

(Figure 5a). An equivalent tiered bioprint was made with three cellular bio-inks incorporating either no cells or hTERT/KER-CT keratinocyte cells labeled with cell mask green or cell mask red. A glass capillary was used to extract a biopsy puncture of the 3D bioprint and the excised artificial tissue was imaged by light sheet microscopy. This imaging revealed a maintained 3D structure, with the different cell-masked stained cell populations residing in the spatial position that was programmed in the 3D print design (Figure 5).

3. Discussion

We present an open-platform 3D bioprinter that represents a low-cost, easily assembled, and operated device for the 3D printing of cells within a hydrogel bio-ink. By using LEGO Mindstorms and simple integrated microfluidics we demonstrate the feasibility of making sophisticated tools, that have the potential to be highly enabling in biological research, from affordable off-the-shelf components. The reported bioprinter is demonstrated in the printing of live keratinocytes and the production of multi-material 3D structures. Cells are shown to remain viable after printing and also after dissolution of the alginate scaffold. The reported bioprinter is able to print multiple bio-inks, either from multiple nozzles operated in parallel, or through the controlled flow of different input bioinks into the droplet generating microfluidic T-junction, via up-stream aqueous flow combiners. The approach is readily scalable, for example in the course of this research we have built three printers for parallel use in different settings and for continuous development. The accessibility of this approach is highlighted here by the contribution of several relatively inexperienced Masters level project students who contributed significantly to the bioprinter design, build, optimization, and coding. In operation the 3D bioprinter

has proved to be a powerful science engagement tool, using the ubiquitous familiar technology of LEGO to produce a sophisticated scientific instrument that is able to provide an accessible introduction to tissue engineering and 3D cell culture study. In this regard, our current focus is the fabrication of human skin models by selectively incorporating and patterning multiple skin cell populations. This could potentially enable mimicry of the heterogeneity and structural complexity of native skin using a bespoke and accessible custom-built 3D bio-printer.

The use of microfluidics in tissue engineering has to-date largely focused on providing a platform for simulating the mechanisms and physiology of organs on the microscale (e.g., organ-on-a-chip or human-on-a-chip) and enabling 3D cell culture.[55–57] Recently, integrating microfluidic-based approaches with 3D bioprinting technologies has shown significant potential in drug testing and the production of more relevant perfused tissue models.[46,57] However, there remain limited reports of continuous flow droplet microfluidic systems being used simultaneously for cell-laden microgel dispensing and as a 3D bio-printing nozzle integrated within a programmable x/y/z platform.[54] The LEGO bioprinter motors have a quoted incremental resolution equivalent to x/y stage movement of ≈4.15 µm. We have systematically evaluated the return movement repeatability following a programmed movement cycle in x, y, and z dimensions over the course of a seven day period measuring a positional return standard deviation of +/− 30.6 µm, consequently currently the droplet size is main determinant of print resolution. Current work is directed toward miniaturization of the bioprinted droplets for 3D printed designs with finer resolution. This can be achieved by reducing the internal diameter of the microfluidics. This will bring printer resolution closer to other methodologies whilst using an alternative multiphase microfluidic approach to droplet generation and cell encapsulation.

A number commercial droplet-based, 3D bio-printing approaches have been developed over the years, which fall into three broad classes comprising; inkjet-based methods using piezo actuation,[38,39] heat actuation,[12,40] or electrostatic forces;[41] microextrusion-based methods using micro-valve dispensing,[42,60] ultrasonic ejection;[43] and finally laser-based ink-melt droplet formation methods.[44,45] Despite the numerous strategies for droplet-based printing, each technique presents recognised limitations resulting in possible cell damage, lack of droplet uniformity, clogging, or challenges with high viscosity or low resolution.[46,47] In-house custom-built 3D bio-printers, or modified commercial fused filament 3D printers to make bioprinters, have been demonstrated in effort to address some of these challenges.[48,58,60,42] These resulting custom-built 3D bio-printers have consisted mainly of programmed cartesian robotic platforms combined with microvalve dispensing systems.[61,62,63] Despite these advances, engineering and programming skills were necessary to develop these in-house built 3D bio-printers, which may hinder wider take-up. The recent advent of low-cost 3D printers, including MakerBot, Ultimaker, FELIXprinters, Maker's Tool Works (MTW), or PrintrBot has encouraged bio-engineers to adapt 3D printers into bio-printers in an attempt to bridge the gap between accessibility and performance.[48,58,60,64] In these cases, the deposition technology is often non-trivial, compared to the simple microfluidic droplet formation reported here, but is generally capable of generating smaller droplet sizes.[60] The multiphase microfluidic approach reported here provides an alternative methodology for simple, low-cost droplet printing that can be readily synchronized with stage movement.[65,66] Whilst adapted 3D printers have not yet achieved the positional precision of commercial high-end bioprinters, recent studies have shown competitive resolutions, with high cell viability and structural integrity, for tissue engineering requirements at low cost.[60,67] A timeline figure and table recapitulating the evolution of custom-built and adapted 3D bio-printers can be found in the Supporting Information Section (S8). The multiphase microfluidic droplet printing approach reported here employed with a LEGO 3D printing platform could be equally applicable to integration with a modified commercial fused filament 3D-printer with the optional development of integrated fluidic and stage control code. Alternatively, the LEGO bioprinter provides a readily accessible and modifiable "kit"-based approach that can be built and assembled with minimal prior engineering expertise. The initial prototype here was developed as a single undergraduate student summer project and subsequent printers may now be built in a day following the supplied instructional video (Video S1, Supporting Information) and parts list (Figure S8, Supporting Information). An operational bioprinter can be built for £550 GBP inclusive of the components for x/y/z printer stage, pumps, and fluidic components, without the need for any additional tools or components (Figure S11, Supporting Information).

Current work is directed toward printing with smaller droplets and alternative bio-inks and their gelation. An anticipated challenge shared with other printing methods is the increase in viscous shear exerted on the encapsulated cells as length scales decrease. Alternative fluidic architectures for droplet formation may facilitate reduced viscous shear by avoiding droplet interaction with the channel walls. Similarly, reduced-viscosity hydrogels that can be gelled by biocompatible processes, whether chemical or physical, will play an important role in furthering these approaches. The use of low-cost and modular microfluidics for droplet generation means fluidics can be readily adapted or replaced for different bio-inks, or different target droplet sizes, as bioprinting needs dictate, and spoiled devices are easily replaced. It is envisaged that through the use of different bio-ink hydrogels, not only can these be used as carriers for different cell types, but also their different chemical and structural properties may be exploited in the resultant printed tissue. Alginate scaffolds may be dissolved by competitive calcium chelation, for example, thus permanent and sacrificial scaffolds can be printed within a single bioprint. The time required and mechanism for structure dissolution is dependent on the print structure volume. It is envisaged that structures could be perfused with sodium citrate followed by PBS solutions, whilst printing, to afford dynamic control of gelation and de-gelling, whilst minimizing cell exposure to dissolution conditions. Such approaches could also provide a valuable mechanism for the creation of conduits within printed tissues that provide a means to perfuse the 3D structure, in a manner comparable of tissue vasculature, to retain cell viability at deeper printing depths. These subjects, together with the development of additional hydrogel bioinks, gelled by alternative mechanisms, are the focus of ongoing study using the presented bioprinting platform.

4. Conclusions

LEGO bricks represent a widely available, cheap, precision-cast engineering tool for the building, and rapid-prototyping of bespoke laboratory equipment. In this case a 3D bioprinter is built which provides an accessible route for biologically focused labs to rapidly and cheaply implement bioprinting techniques. The universality of LEGO as a design-and-build tool, together with the ability to readily share design builds, along with possibilities for user enhancement and customization, provides powerful opportunities for democratization of scientific instrumentation. Likewise, such systems can serve as highly functional prototypes that can easily be redesigned and reconfigured before operational limits are pushed further with more traditional workshop builds informed by LEGO prototypes. This is the focus of ongoing work. These prototypes may be repurposed as demonstrators, or the components built into new tools. Similarly, functional LEGO laboratory tools represent engaging and accessible learning opportunities for students, (as we have found in the course of this work), and can serve as a rich engagement and outreach experience for science communication, not only providing a familiar route into a new scientific area, but also showcasing the accessibility of science and the role of creativity in research. Indeed, modular construction toys represent a unique and bespoke route to the construction of diverse machines.[2–4,68] The use of LEGO as a tool in scientific research has been the subject of recent review, highlighting its ability to fulfil specific scientific requirements and create professional-grade tools and systems that can be made available to all researchers regardless of financial and technological constraints.[69]

5. Experimental Section

LEGO Build (see Supporting Information and Video): The 3D bio-printer design used in this study consisted of two main components: A low-cost three-axis programmable motorized LEGO platform combined with a microfluidic T-junction droplet generator device connected to a dual syringe infusion only pump (KD Scientific) or LEGO syringe driver system.

The programmable x/y/z stage was constructed from a combination of LEGO Technic and the LEGO Mindstorms EV3 LEGO including modular motors, sensors, actuators, and a control brick. The required LEGO components were purchased from several sources (LEGO Store, Cardiff; Ebay). The design of the x/y/z stage was based on one originally reported on the Instructables website that held a polymer extrusion pen to make a traditional plastic 3D printer.[53]

Printer Control: The programming software used to generate orders to the motorized platform used a visual programming language (VPL) powered by LabVIEW (LEGO Mindstorms Programmer). The programmes consisted of a chain of command blocks and arrows (or graphic symbols) that were uploaded and executed through the "programmable brick". These programmes dictated the movements of the stage in the x, y, and z plane at defined trajectories and speeds. In brief, the stage speed, trajectory, and distance were user-definable and programmed to work in unison with the frequency of droplet production. This allowed controlled printing resolution and dimensionality.

Microfluidic Droplet Production: Alginate droplets were generated by means of a droplet-based microfluidic T-junction device (Kinesis, SUPELCO). Glacial acetic acid in mineral oil (SIGMA) was continuously delivered into one channel as the continuous oil phase, whereas the aqueous phase or alginate/calcium carbonate solution was delivered into the opposite channel (aqueous phase). Both phases were delivered via 3 mL plastic syringes with a diameter of 8.66 mm. The interfacial tension between the two immiscible phases created consistent monodisperse water-in-oil droplets. Subsequently, alginate droplets were gelled downstream of the T-junction via ionic cross-linking with bivalent calcium ions.[7,54,55] The liquid materials were pumped using a dual syringe infusion only pump (KDScientific) at the desired flow rates (ml/hr).

Optimisation of Printing Parameters: The printer bed was leveled with a digital spirit level on a smart phone and printing was performed into a Petri dish containing 20 ml of mineral oil. Printing was performed onto a glass coverslip placed at the bottom of the dish. The printer was programmed to print four parallel lines at a z-axis height of 1.12 mm above the glass coverslip. Flow rates ranged from 2–10 mL hr^{-1} and printer movement speeds of 0.47–5.00 mm s^{-1} were employed in the combinations illustrated in Figure 4.

Cell Culture: All cell culture procedures were performed in a class 2 biosafety cabinet (BSL-II) using 70% ethanol as a disinfectant to maintain aseptic conditions. Cells were maintained in an incubator at 37 °C containing 5% CO_2.

HaCaT cell lines (purchased from ATCC cultured in Dulbecco's modified Eagle medium (DMEM)- GlutaMAX (high glucose supplement) supplemented with 10% foetal bovine serum (FBS) (Biowest #S1810-500) and 1% penicillin-streptomycin. DMEM-GlutaMAX contains 4 mM of L-glutamine and 1.8 mM of calcium ions by default.

Prior to cell confluency, the culture medium was aspirated, and cells were washed twice with sterile phosphate buffer saline (PBS). Cells were then detached from the surface of the cell culture flask by adding 0.25% trypsin-EDTA and incubating at 37 °C for 5–10 min. The flask was then lightly tapped with the palm of the hand until they became rounded and fully detached. The cell suspension was transferred into a 15 mL tube containing fresh cell culture medium with FBS. The cells were then centrifuged at 300 × g for 5 min. After discarding the supernatant, the cell pellet was re-suspended in fresh cell culture medium and re-seeded with adequate cell densities in new cell culture flasks. Sub-cultivation ratios ranged between 1/5 to 1/10 for routine cell culture or other desired ratios as per experimental requirements. Cell culture medium was renewed every 2–3 days. The volumes of reagents used were scaled according to the tissue culture flask size.

hTERT/KER-CT keratinocyte cells (purchased from ATCC) were sub-cultured similar to HaCaT cells with few modifications. hTERT cells were cultured in the KGM Gold Keratinocyte Growth Medium Bulletkit supplemented with 0.50 mL hydrocortisone, 0.50 mL transferrin, 0.25 mL epinephrine, 0.50 mL Gentamicin sulfate-Amphotericin (GA-1000), 2 mL, Bovine Pituitary Extract (BPE), 0.50 mL human Epidermal Growth Factor (hEGF), and 0.50 mL insulin. hTERT cells were detached using 0.05% trypsin-EDTA and incubating at 37 °C for 10 min.

Determining Cell Count and Viability: An equal flow rate of oil to alginate phase of 4 mL hr^{-1} was used to generate cell-laden droplets. HaCaT cells were either seeded at a 150000-cell density per well in a 6 well plate for the control condition in 2D culture, or 3D bio-printed in alginate droplets to yield approximately the same number of cells per well. A cell density of 106 cells mL^{-1} was mixed in the alginate/calcium carbonate/DMEM solution, and an equal flow rate of 4 mL/hr was used. To generate 150000 cells per well, a final extrusion volume of 150 µL per well was determined. Therefore, a continuous extrusion time of ≈13.5 s per well was carried out. HaCaT cells were 3D bio-printed in sterile mineral oil which was directly removed after extrusion, and the cell-laden droplets were washed and maintained in culture medium at 37 °C and 5% CO_2 in an incubator. Cell-laden alginate droplets were incubated in a filter sterilised solution of 250 mM Ethylenediaminetetraacetic acid (EDTA) and PBS for 15 min for complete droplet dissolution and cell liberation. The cells were transferred to a 15 mL falcon tube with fresh DMEM and centrifuged at 1200 rpm for 5 min. The supernatant was discarded, and the cells were resuspended in 5 mL of fresh DMEM. Cell viability was assessed by counting the number of viable and dead cells using the trypan blue exclusion method.[50] For the 2D culture control condition, the 2D HaCaT monolayer was detached with trypsin

(0.25%)-EDTA (0.9 mM) with a 15 min incubation, before an equivalent cell reclamation procedure and trypan blue assay for cell viability assessment.

Experimental Bioprinting: For cell encapsulation, an alginate-media (DMEM) solution was prepared using cell culture media instead of deionized water. Calcium-free DMEM was supplemented with 1% penicillin-streptomycin-glutamine (PSG). The alginate-DMEM solution was stirred for 2 h at room temperature. The plastic syringes used were sterile and disposable. HaCaT cells were detached, suspended in culture medium, and counted using a haemocytometer. The cells were centrifuged and re-suspended at a density of 10 million cells per ml of the alginate-DMEM solution.

Cell culture and preparation for encapsulation used comparable protocols to previous studies, with a few modifications.[7] Monodisperse alginate droplets containing HaCaT cells were generated using a microfluidic device and extruded in a 60 mm petri dish containing sterile mineral oil. After bio-printing, the sterile mineral oil was removed, and the cell-laden hydrogel droplets were washed twice with PBS then kept in culture medium at 37° and 5% CO_2 in an incubator.

15 µm polystyrene fluorescent microspheres or FluoSpheres in 4 different colors (carmine, green, yellow, and red-orange) were purchased from ThermoFisher. FluoroSpheres were centrifuged at 1200 rpm for 5 min then mixed with the alginate solution for a final concentration of 5×10^5 beads per mL. This solution was then used to generate FluoroSphere-encapsulated droplets of different colours.

Imaging Droplets: Phase contrast and brightfield images of HaCaT-encapsulated alginate droplets were captured using an IX70 Olympus Inverted Phase Contrast Microscope (Olympus) Prior to encapsulation, HaCaT cells were fluorescently labeled with a Live/Dead stain (ab115347 – abcam) for confocal microscopy visualization. The staining solution was a mixture of two fluorescent dyes: The live cell dye that labels viable cells green and the dead cell dye labelling dead cells red. The green fluorescent dye was membrane permeant and produces green fluorescence only following enzymatic activity in viable cells. The red dye only penetrates dead cells with compromised plasma membranes and produces red fluorescence upon binding to the DNA.

Once detached with trypsin from the flask, HaCaT cells were washed with PBS and DMEM (to neutralize any remaining trypsin), counted, and centrifuged at 1200 rpm. The supernatant was discarded, and the cells were incubated with the Live/Dead stain in the dark at a working solution of 10× in sterile PBS for 10 min. Then, HaCaT cells were washed three times by centrifuging, discarding the supernatant and adding sterile PBS. After the final wash, the PBS was discarded, and the cells were re-suspended in a sterile alginate/calcium carbonate/DMEM solution at a final cell density of 10^7 cells mL^{-1}. The cell solution was transferred to a sterile 3 mL syringe for subsequent cell encapsulation with the microfluidic device and syringe driver.

Fluorescently encapsulated HaCaT cells were visualized using the Confocal Zeiss LSM (Laser Scanning Microscopy) 880 with a 10× objective. The excitation wavelengths used for the Live and Dead dyes were 495 and 528 nm respectively. Optical slices of 10 µm thickness in the z-axis were taken using the full z-penetrance distance of the confocal microscope lasers. Images were captured on the Zeiss ZEN software and further analyzed using Image J,[51] (Fiji distribution),[52] for 3D reconstitution and grouped z projection.

Imaging Cell Encapsulated Tissues via Lightsheet Microscopy: hTERT/KER-CT cells were stained with CellMask Deep Red Plasma Membrane Stain (Thermo) or with Green CellMask (Thermo) before encapsulation and re-suspended in an alginate/$CaCO_3$/DMEM solution at a cell density of 10^7 cells mL^{-1} each.

Light Sheet Fluorescent Microscopy (Zeiss Lightsheet z. 1) was an optical method that requires samples to be either embedded in a transparent polymer or suspended in a capillary with a refractive index of 1 (i.e., FEP (Fluorinated Ethylene Propylene) tubes). The sample was then suspended in a liquid filled chamber with two illumination objectives exciting a focal plane from the sides. The fluorescent emission was detected by a separated detection objective. To prepare the polymer, a solution of 1% low melting point agarose (Thermo) was prepared in deionized water. Cell-encapsulated droplets were printed and maintained at 37 °C in culture medium. When it reached 37 °C, a few cell-encapsulated droplets were mixed in the agarose solution. A small volume of melted agarose and cell-laden droplets were subsequently aspirated using a piston into a glass capillary of 1.5 mm diameter. Once completely solidified within the tube, the embedded droplets were pushed into the light sheet chamber for image acquisition. A magnification of 5× was used with excitation wavelengths for the Live and Dead dyes at 495 and 528 nm, respectively. Optical slices of 10 µm were taken for the full length of the glass capillary. The Zeiss ZEN software was utilized to visualize the cell-laden droplets and 3D reconstitution/grouped Z projection was carried out using Image J,[51] (Fiji distribution).[52]

Glass capillary devices did not allow for long term hold of full 3d bio-printed structures due to the large size of the structure. A custom-made device to optimize sample entrapment and sample bio-punching were fashioned using a FEP tubing instead (Figure S5, Supporting Information). This consisted of a 1 mL plastic syringe attached to a 4 and 3 mm external and internal diameter FEP tube, respectively. The syringe ensured optimal vacuum action on the bio-punched sample whilst the FEP tube serves as a transparent polymer that had a similar refractive index to water, making it a suitable alternative to glass. Parafilm held both objects together to prevent air from escaping. A razor-sharp seamless cutting tip (4 mm diameter) removed from a bio-punch device (REF) was connected to the end of the FEP tube to optimize sample bio-punch. Alternatively, the end of the FEP tube was sharpened using a pencil sharpener. Both allowed to take a biopsy and subsequently extract the sample into the FEP tube. A sample from the 3D-bioprinted construct was taken using the custom-made syringe/FEP/bio-punch device and was entrapped in the FEP tube (Figure S5, Supporting Information). The entire device was inserted into the liquid filled chamber for image acquisition. A magnification of 5× was used with excitation wavelengths for the Green and Deep Red CellMask dyes at 495 and 528 nm, respectively. Optical slices of 10–15 µm were taken for the full length of the FEB tube. The Zeiss ZEN software was utilized to visualize the cell-laden droplets and 3D reconstitution/grouped Z projection was carried out using Image J.

Macro-Scale Imaging: Macroscopic images of 3D bio-printed structures containing different coloured FluoSpheres were taken using a Nikon SMZ 745T (Nikon) stereoscope. A Brunel Eyecam Plus (Brunel Microscopes Ltd) was used to visualize the bio-printed construct and images were saved through the SharpCap capture tool program. Image analysis was carried out using Image J,[51] (Fiji distribution).[52]

Printer Mechanical Reproducibility: Camera images captured nozzle location repeatability contacting a 1 × 1 mm square matrix location grid serving as a reference graticule. The printer was programmed to perform a series of lateral and vertical movements before lowering in z. This procedure was imaged and repeated between 6 and 13 times on three separate days over the course of one week. A total of 31 runs were captured and analyzed using Image J,[51] (Fiji distribution)[52] to determine nozzle location against the reference grid using four measurements for each run. An image montage of each run was included in the Supporting Information.

Supporting Information

Supporting Information is available from the Wiley Online Library or from the author.

Acknowledgements

This work was primarily supported by a British Skin Foundation (BSF) PhD studentship grant (grant number: 059/s/16), together with support from H2020- EU.1.2.2. – FET Proactive Grant agreement ID: 824060 – "ACDC", Cardiff Institute for Tissue Engineering and Repair (CITER),

The Cardiff Undergraduate Research Opportunities Programme (CUROP) and Cardiff University Tissue Engineering and Regenerative Medicine M.Sc and M.Pharm student project schemes. The authors would like to acknowledge the support of Dr. Anthony Hayes and Dr. Peter Watson for providing support, training, and practice for the light sheet fluorescent microscopy platform alongside assisting with custom method development for bio-tissue imaging. The authors would like to acknowledge the help of Iestyn Jones for the cooperation in the subculture of cell lines when required.

Conflict of Interest

The authors declare no conflict of interest.

Author Contributions

C.T., S.C., and O.K.C. conceived the project and secured funding. A.M., C.T., S.C., and O.K.C. supervised the research. A.M. led cell culture, cell characterization, cell bioprinting, bio-printer application and bioprint characterization laboratory work, as well as providing project guidance and strategic alignment with A.M.'s wider doctoral research. J.L. contributed microfluidic designs made by 3D fused-filament printing. A.M. contributed to all experimental work. O.K.C., A.M., C.T., and S.C. wrote the manuscript. All authors contributed in the discussion and analysis of results. The following contributions were made by undergraduate students: K.H. built the initial prototype printer, K.S. contributed to print parameter characterization, C.P. and E.R. contributed to Mindstorms and Labview coding respectively. S.M. and A.A. contributed to characterizing gelation and dissolution conditions along with G.McD. D.J. contributed to building and evaluating printing with LEGO microfluidic pumps, P.C.-W. contributed to multi-nozzle and multi-material printing. G.McD. and L.E. contributed to time-lapse printer builds and bioprint characterization.

Data Availability Statement

The data that support the findings of this study are available from the corresponding author upon reasonable request.

Keywords

3D bioprinting, lego, microfluidics, tissue engineering

Received: July 30, 2022
Revised: October 19, 2022
Published online:

[1] N. Shahrubudin, T. Lee, R. Ramlan, *Procedia Manuf* **2019**, *35*, 1286.
[2] R. Moser, G. Kettlgruber, C. Siket, M. Drack, I. Graz, U. Cakmak, Z. Major, M. Kaltenbrunner, S. Bauer, *Adv. Sci.* **2016**, *3*, 1500396.
[3] L. Gerber, A. Calasanz-Kaiser, L. Hyman, K. Voitiuk, U. Patil, I. Riedel-Kruse, *PLoS Biol.* **2017**, *15*, e2001413.
[4] P. Almada, P. Pereira, S. Culley, G. Caillol, F. Boroni-Rueda, C. Dix, G. Charras, B. Baum, R. Laine, C. Leterrier, R. Henriques, *Nat. Commun.* **2019**, *10*, 1223.
[5] J. Fernsler, V. Nguyen, A. Wallum, N. Benz, M. Hamlin, J. Pilgram, H. Vanderpoel, R. Lau, *Am. J. Phys.* **2017**, *85*, 655.
[6] F. Quercioli, B. Tiribilli, A. Mannoni, S. Acciai, *Appl. Opt.* **1998**, *37*, 3408.
[7] A. Morgan, L. Hidalgo San Jose, W. Jamieson, J. Wymant, B. Song, P. Stephens, D. Barrow, O. Castell, *PLoS One* **2016**, *11*, 0152023.
[8] C. Owens, A. Hart, *Lab Chip* **2018**, *18*, 890.
[9] A. Dababneh, I. Ozbolat, *J. Manuf. Sci. Eng.* **2014**, *136*, 061016.
[10] L. Moroni, T. Boland, J. Burdick, C. De Maria, B. Derby, G. Forgacs, J. Groll, Q. Li, J. Malda, V. Mironov, C. Mota, M. Nakamura, W. Shu, S. Takeuchi, T. Woodfield, T. Xu, J. Yoo, G. Vozzi, *Trends Biotechnol.* **2018**, *36*, 384.
[11] Z. Xia, S. Jin, K. Ye, *SLAS TECHNOLOGY: Translating Life Sciences Innovation* **2018**, *23*, 301.
[12] S. Murphy, A. Atala, *Nat. Biotechnol.* **2014**, *32*, 773.
[13] L. Gao, M. Kupfer, J. Jung, L. Yang, P. Zhang, Y. Da Sie, Q. Tran, V. Ajeti, B. Freeman, V. Fast, P. Campagnola, B. Ogle, J. Zhang, *Circ. Res.* **2017**, *120*, 1318.
[14] H. Kang, S. Lee, I. Ko, C. Kengla, J. Yoo, A. Atala, *Nat. Biotechnol.* **2016**, *34*, 312.
[15] T. Baltazar, J. Merola, C. Catarino, C. Xie, N. Kirkiles-Smith, V. Lee, S. Hotta, G. Dai, X. Xu, F. Ferreira, W. Saltzman, J. Pober, P. Karande, *Tissue Eng., Part A* **2020**, *26*, 227.
[16] R. Pedde, B. Mirani, A. Navaei, T. Styan, S. Wong, M. Mehrali, A. Thakur, N. Mohtaram, A. Bayati, A. Dolatshahi-Pirouz, M. Nikkhah, S. Willerth, M. Akbari, *Adv. Mater.* **2017**, *29*, 1606061.
[17] B. Kim, G. Gao, J. Kim, D. Cho, *Adv. Healthcare Mater.* **2018**, *8*, 1801019.
[18] J. Albritton, J. Miller, *Dis. Models Mech.* **2017**, *10*, 3.
[19] R. Wang, Y. Wang, B. Yao, T. Hu, Z. Li, S. Huang, X. Fu, *Int. Wound J.* **2018**, *16*, 134.
[20] L. Moroni, J. Burdick, C. Highley, S. Lee, Y. Morimoto, S. Takeuchi, J. Yoo, *Nat. Rev. Mater.* **2018**, *3*, 21.
[21] S. England, A. Rajaram, D. Schreyer, X. Chen, *Int. J. Bioprint.* **2017**, *5*, 1.
[22] X. Ma, J. Liu, W. Zhu, M. Tang, N. Lawrence, C. Yu, M. Gou, S. Chen, *Adv. Drug Delivery Rev.* **2018**, *132*, 235.
[23] C. Tomasina, T. Bodet, C. Mota, L. Moroni, S. Camarero-Espinosa, *Materials* **2019**, *12*, 2701.
[24] D. Kolesky, K. Homan, M. Skylar-Scott, J. Lewis, *Proc. Natl. Acad. Sci. USA* **2016**, *113*, 3179.
[25] M. Kim, B. Chi, J. Yoo, Y. Ju, Y. Whang, I. Chang, *PLoS One* **2019**, *14*, 0223689.
[26] B. Knörlein, D. Baier, S. Gatesy, J. Laurence-Chasen, E. Brainerd, *J Exp Biol* **2016**, *219*, 3701.
[27] L. Hidalgo San Jose, P. Stephens, B. Song, D. Barrow, *Tissue Eng., Part C* **2018**, *24*, 158.
[28] T. Tran, F. Lan, C. Thompson, A. Abate, *J. Phys. D: Appl. Phys.* **2013**, *46*, 114004.
[29] D. Baxani, A. Morgan, W. Jamieson, C. Allender, D. Barrow, O. Castell, *Angew. Chem., Int. Ed.* **2016**, *55*, 14240.
[30] J. Li, D. Baxani, W. Jamieson, W. Xu, V. Rocha, D. Barrow, O. Castell, *Adv. Sci.* **2019**, *7*, 1901719.
[31] H. Song, J. Tice, R. Ismagilov, *Angew. Chem.* **2003**, *115*.
[32] O. Castell, C. Allender, D. Barrow, *Lab Chip* **2008**, *8*, 1031.
[33] B. Chueh, Y. Zheng, Y. Torisawa, A. Hsiao, C. Ge, S. Hsiong, N. Huebsch, R. Franceschi, D. Mooney, S. Takayama, *Biomed. Microdevices* **2009**, *12*, 145.
[34] B. Barnett, P. Gailloud, *Journal of Vascular and Interventional Radiology* **2011**, *22*, 203.
[35] Z. Wu, X. Su, Y. Xu, B. Kong, W. Sun, S. Mi, *Sci. Rep.* **2016**, *6*, 24474.
[36] O. Castell, *Microfluidic devices for continuous liquid-liquid-solid chemical extractions*, Cardiff University, XX September **2008**.
[37] C. Lucy, F. Cantwell, *Anal. Chem.* **1989**, *61*, 101.
[38] R. Saunders, J. Gough, B. Derby, *Biomaterials* **2008**, *29*, 193.
[39] J. Li, M. Chen, X. Fan, H. Zhou, *J Transl Med* **2016**, *14*, 271.
[40] X. Cui, T. Boland, D. D. D'Lima, M. K. Lotz, *Recent Pat. Drug Deliv. Formul.* **2012**, *6*, 149.

[41] S. Kamisuki, T. Hagata, C. Tezuka, Y. Nose, M. Fujii, M. Atobe, presented at *IEEE Eleventh Annual International Workshop on Micro Electro Mechanical Systems*, Heidelberg, Germany **1998**.
[42] A. Faulkner-Jones, C. Fyfe, D. Cornelissen, J. Gardner, J. King, A. Courtney, W. Shu, *Biofabrication* **2015**, *7*, 044102.
[43] J. Meacham, M. Varady, F. Degertekin, A. Fedorov, *Phys. Fluids* **2005**, *17*, 100605.
[44] J. Barron, P. Wu, H. Ladouceur, B. Ringeisen, *Biomed. Microdevices* **2004**, *6*, 139.
[45] V. Keriquel, H. Oliveira, M. Rémy, S. Ziane, S. Delmond, B. Rousseau, S. Rey, S. Catros, J. Amédée, F. Guillemot, J. Fricain, *Sci. Rep.* **2017**, *7*, 1778.
[46] W. Peng, D. Unutmaz, I. Ozbolat, *Trends Biotechnol.* **2016**, *34*, 722.
[47] H. Gudapati, M. Dey, I. Ozbolat, *Biomaterials* **2016**, *102*, 20.
[48] J. Reid, P. Mollica, G. Johnson, R. Ogle, R. Bruno, P. Sachs, *Biofabrication* **2016**, *8*, 025017.
[49] M. Kahl, M. Gertig, P. Hoyer, O. Friedrich, D. Gilbert, *Frontiers in Bioengineering and Biotechnology* **2019**, *7*, 00184.
[50] W. Strober, *Curr. Protoc. Immunol.* **2015**, *111*, A3B1.
[51] C. Schneider, W. Rasband, K. Eliceiri, *Nat. Methods* **2012**, *9*, 671.
[52] J. Schindelin, I. Arganda-Carreras, E. Frise, V. Kaynig, M. Longair, T. Pietzsch, S. Preibisch, C. Rueden, S. Saalfeld, B. Schmid, J. Tinevez, D. White, V. Hartenstein, K. Eliceiri, P. Tomancak, A. Cardona, *Nat. Methods* **2012**, *9*, 676.
[53] www.instructables.com/3D-Printer-With-Lego-EV3/. Accessed 17 May **2021**.
[54] L. Serex, A. Bertsch, P. Renaud, *Micromachines* **2018**, *9*, 86.
[55] W. Tan, S. Takeuchi, *Adv. Mater.* **2007**, *19*, 2696.
[56] S. Utech, R. Prodanovic, A. Mao, R. Ostafe, D. Mooney, D. Weitz, *Adv. Healthcare Mater.* **2015**, *4*, 1628.
[57] S. Lee, S. Jin, Y. Kim, G. Sung, J. Chung, J. Sung, *Biomed. Microdevices* **2017**, *19*, 22.
[58] A. Graham, S. Olof, M. Burke, J. Armstrong, E. Mikhailova, J. Nicholson, S. Box, F. Szele, A. Perriman, H. Bayley, *Sci. Rep.* **2017**, *7*, 7004.
[59] L. Zhou, A. Wolfes, Y. Li, D. Chan, H. Ko, F. Szele, H. Bayley, *Adv. Mater.* **2020**, *32*, 2002183.
[60] N. Okubo, A. Qureshi, K. Dalgarno, K. Goh, S. Derebail, *Int. J. Bioprint.* **2019**, *13*, e00043.
[61] W. Lee, J. C. Debasitis, V. K. Lee, J.-H. Lee, K. Fischer, K. Edminster, J.-K. Park, S.-S. Yoo, *Biomaterials* **2009**, *30*, 1587.
[62] F. Xu, S. J. Moon, A. E. Emre, E. S. Turali, Y. S. Song, S. A. Hacking, J. Nagatomi, U. Demirci, *Biofabrication* **2010**, *2*, 014105.
[63] G. Villar, A. D. Graham, H. Bayley, *Science* **2013**, *340*, 48.
[64] N. Bessler, D. Ogiermann, M.-B. Buchholz, A. Santel, J. Heidenreich, R. Ahmmed, H. Zaehres, B. Brand-Saberi, *HardwareX* **2019**, *6*, e00069.
[65] C. Colosi, M. Costantini, R. Latini, S. Ciccarelli, A. Stampella, A. Barbetta, M. Massimi, L. Conti Devirgiliis, M. Dentini, *J. Mater. Chem. B* **2014**, *2*, 6779.
[66] C. Colosi, S. Shin, V. Manoharan, S. Massa, M. Costantini, A. Barbetta, M. Dokmeci, M. Dentini, A. Khademhosseini, *Adv. Mater.* **2015**, *28*, 677.
[67] A. Sanz-Garcia, E. Sodupe-Ortega, A. Pernía-Espinoza, T. Shimizu, C. Escobedo-Lucea, *Polymers* **2020**, *12*, 1734.
[68] D. Schmieden, S. Basalo Vázquez, H. Sangüesa, M. van der Does, T. Idema, A. Meyer, *ACS Synth. Biol.* **2018**, *7*, 1328.
[69] E. Boulter, J. Colombelli, R. Henriques, C. C. Féral, *Trends Biotechnol.* **2022**, *40*, 1073.